ORIGINAL ARTICLE

Vanishing white matter: Eukaryotic initiation factor 2B model and the impact of missense mutations

Inna Slynko[1] | Stephanie Nguyen[2] | Eline M. C. Hamilton[3] | Lisanne E. Wisse[3] | Iwan J. P. de Esch[1] | Chris de Graaf[1] | John B. Bruning[2] | Christopher G. Proud[4,5] | Truus E. M. Abbink[3] | Marjo S. van der Knaap[3,6]

[1]Division of Medicinal Chemistry, Amsterdam Institute for Molecules, Medicines and Systems, Vrije Universiteit Amsterdam, Amsterdam, the Netherlands

[2]Institute for Photonics and Advanced Sensing (IPAS), School of Biological Sciences, The University of Adelaide, Adelaide, SA, Australia

[3]Department of Child Neurology, Emma Children's Hospital, Amsterdam University Medical Centers, Vrije Universiteit and Amsterdam Neuroscience, Amsterdam, the Netherlands

[4]Hopwood Centre for Neurobiology and Lifelong Health Theme, South Australian Health & Medical Research Institute, Adelaide, SA, Australia

[5]School of Biological Sciences, The University of Adelaide, Adelaide, SA, Australia

[6]Department of Functional Genomics, Amsterdam Neuroscience, VU University, Amsterdam, the Netherlands

Correspondence
Marjo S. van der Knaap, Department of Child Neurology, Amsterdam University Medical Centers, Location VU University Medical Center, De Boelelaan 1117, 1081 HV Amsterdam, the Netherlands.
Email: ms.vanderknaap@amsterdammumc.nl

Present address
Inna Slynko, Grünenthal GmbH, Aachen, 52078, Germany
Chris de Graaf, Christopher G. Proud and Truus E. M. Abbink, Sosei Heptares, Steinmetz Building, Granta Park, Great Abington, Cambridge, CB21 6DG, UK

Funding information
ZonMw, Grant/Award Number: TOP grant 91211005; Nederlandse Organisatie voor Wetenschappelijk Onderzoek (NWO), Grant/Award Number: TOPPUNT 718.014.002

Abstract

Background: Vanishing white matter (VWM) is a leukodystrophy, caused by recessive mutations in eukaryotic initiation factor 2B (eIF2B)-subunit genes (*EIF2B1–EIF2B5*); 80% are missense mutations. Clinical severity is highly variable, with a strong, unexplained genotype–phenotype correlation.

Materials and Methods: With information from a recent natural history study, we severity-graded 97 missense mutations. Using in silico modeling, we created a new human eIF2B model structure, onto which we mapped the missense mutations. Mutated residues were assessed for location in subunits, eIF2B complex, and functional domains, and for information on biochemical activity.

Results: Over 50% of mutations have (ultra-)severe phenotypic effects. About 60% affect the ε-subunit, containing the catalytic domain, mostly with (ultra-)severe effects. About 55% affect subunit cores, with variable clinical severity. About 36% affect subunit interfaces, mostly with severe effects. Very few mutations occur on the external eIf2B surface, perhaps because they have minor functional effects and are tolerated. One external surface mutation affects eIF2B-substrate interaction and is associated with ultra-severe phenotype.

Conclusion: Mutations that lead to (ultra-)severe disease mostly affect amino acids with pivotal roles in complex formation and function of eIF2B. Therapies for VWM

Inna Slynko, Stephanie Nguyen, Eline M. C. Hamilton contributed equally to this work.

Marjo S. van der Knaap shared senior authorship with Christopher G. Proud and Truus E.M. Abbink.

----

are emerging and reliable mutation-based phenotype prediction is required for propensity score matching for trials and in the future for individualized therapy decisions.

1 | INTRODUCTION

Vanishing white matter (VWM; OMIM 603896) is a leukodystrophy with highly variable severity, ranging from antenatal onset, rapidly fatal disease to adult onset, and mild disease with slow progression (Labauge et al., 2009; van der Knaap et al., 2003, 2006). Age of onset is the only consistent independent clinical predictor for overall disease severity (Fogli, Schiffmann, Bertini, et al., 2004; Hamilton et al., 2018).

VWM is caused by recessive mutations in any of the five genes *EIF2B1–5* (OMIM 606686, 606454, 606273, 606687, 603945, respectively), encoding the α- to ε-subunits of eukaryotic initiation factor 2B (eIF2B) (Leegwater et al., 2001; van der Knaap et al., 2002). eIF2B is indispensable for the initiation of translation of mRNAs into proteins (Dever, 2002; Pavitt, 2005). It is the guanine nucleotide exchange factor (GEF) for initiation factor eIF2. eIF2-GTP and initiator-tRNA form the "ternary complex" that scans the mRNA for the translation start codon. When translation starts, eIF2 dissociates in an inactive GDP-bound form. eIF2B recycles eIF2-GDP to eIF2-GTP, thereby "reactivating" it for the next round of translation (Williams et al., 2001). Inhibition of eIF2B mediates the downregulation of protein synthesis under stress. Various stressors activate different kinases that phosphorylate eIF2α; phosphorylated eIF2α inhibits eIF2B (Proud, 2005; Rowlands et al., 1988). eIF2B is a hetero-decameric complex containing two copies of all subunits (Gordiyenko et al., 2014; Wortham et al., 2014). The γ- and ε-subunits form the catalytic subcomplex; the α-, β-, and δ-subunits constitute the regulatory subcomplex (please see Figure 1 for details of the structure of human eIF2B) (Gomez & Pavitt, 2000; Liu et al., 2011; Reid et al., 2012; Wang et al., 2012).

Missense mutations are the most common mutation type in VWM, comprising 80% of total (van der Knaap et al., 2010). They impact eIF2B in diverse ways, including impaired complex formation, complex instability, impaired binding to the substrate eIF2, and decreased catalytic (GEF) activity (Li et al., 2004; Liu et al., 2011; Leng et al., 2011; Matsukawa et al., 2011; Wang et al., 2012; Wortham & Proud, 2015). Mutations most often decrease eIF2B's GEF activity in cell-based assays (Fogli, Schiffmann, Hugendubler, et al., 2004; Horzinski et al., 2009; Leng et al., 2011; Li et al., 2004; Liu et al., 2011). Against expectations, no clear correlation between residual eIF2B GEF activity measured in vitro and clinical disease severity has emerged (Liu et al., 2011),

contrasting with an evident genotype–phenotype correlation (Fogli, Schiffmann, Bertini, et al., 2004; van der Lei et al., 2010). In the case of compound heterozygosity for two different missense mutations, they co-determine the phenotype (van der Lei et al., 2010).

In 2016, the first three-dimensional structure of a decameric eIF2B complex was described for *Schizosaccharomyces pombe* (*S. pombe*) (Kashiwagi et al., 2016). In 2018, two structures of a human eIF2B decamer were released (Tsai et al., 2018; Zyryanova et al., 2018). Both contain many gaps. A separate structure of the human catalytic domain was determined (Boesen et al., 2004; Wei et al., 2010), but structural information regarding the connection with the rest of eIF2Bε is lacking.

Homology or comparative modeling is a method to construct an atomic-resolution model structure of a protein from its amino acid sequence and the known three-dimensional structure of a related, homologous protein, the "template." To build a high-quality model, one or more reliable template structures are needed. Higher similarity between query and template protein results in better alignment and more accurate model. Usually sequence identity of more than 30% is considered sufficient to build a tertiary protein structure (Dolan et al., 2012; Fiser, 2010), while for reliable placement of flexible loops and side-chains higher similarity is needed (Wallner & Elofsson, 2005).

We analyzed missense mutations of VWM patients and graded their severity based on clinical phenotype. We built a comprehensive model for human eIF2B using the three available template structures and applied modeling to fill the many structural gaps. We mapped the severity-graded mutations onto the new model and assessed the links between VWM disease severity and determinants at molecular level, that is, location of each single mutation relative to others and their potential roles in the assembly or stability of eIF2B heterodecameric complexes, interactions with eIF2 and catalytic function.

2 | MATERIALS AND METHODS

2.1 | Ethical compliance

With approval of the ethics committee of the VU University Medical Center, Amsterdam, and written informed consent from participating patients or guardians, we performed a
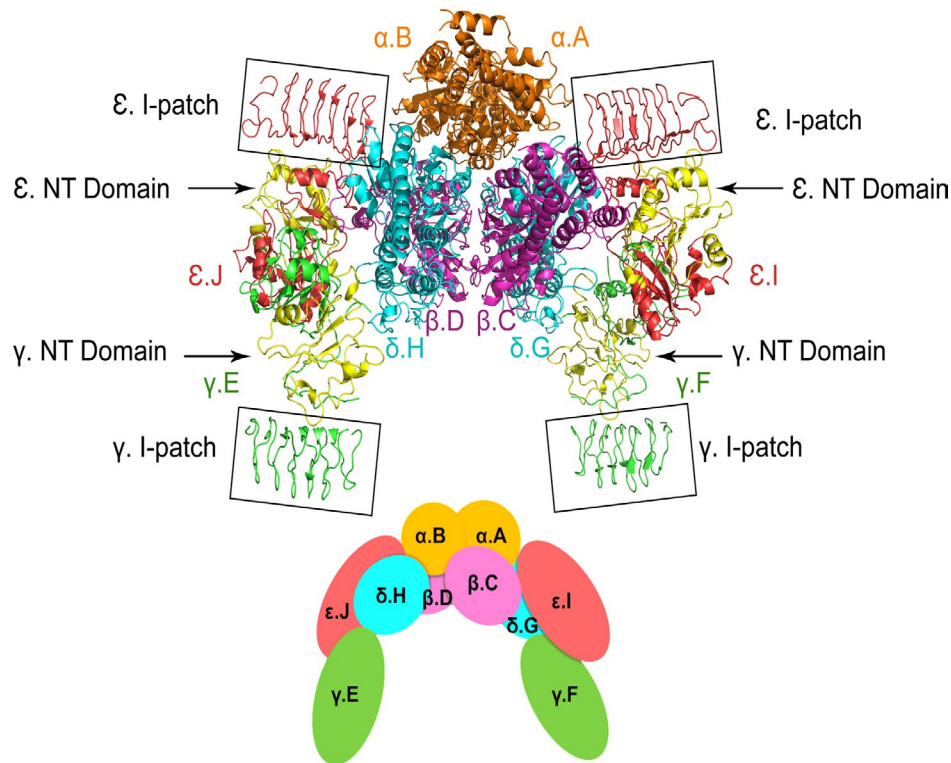
FIGURE 1 Schematic homology structure of human eIF2B. The structure of the human eIF2B complex is shown as cartoon representation, where each of the subunits has the same color as in the schematic representation in the inset. The 10 chains are named alphabetically from A to J, corresponding to the chain names in the template structure (PDB code: 5B04). The eIF2B decamer consists of regulatory (α, β, δ) and catalytic (γ, ε) subcomplexes. The γ- and ε-subunits share two homologous domains, which show sequence similarities with nucleotidyl transferases (NT domain, shown as yellow ribbon in ε- and γ-subunits) and acyl transferases. The acyl transferases contain so-called I-patch repeats, which have approximate hexad spacing of the hydrophobic branched-chain amino acids isoleucine (Ile), valine (Val), and leucine (Leu). The I-patch domain and NT domain alone do not interact with other subunits, but certain mutations or disruptions within them do impact on the formation of eIF2B holo-complexes. Two neighboring amino acids at positions 263–264 in eIF2Bε, asparagine (Asn or N), and phenylalanine (Phe or F), form the NF motif that is important for eIF2B catalytic function. The catalytic domain is not represented in this figure because its spatial orientation is unknown. It is located toward the C-terminus of eIF2Bε, while the far C-terminal region contains conserved acidic and aromatic residues, which are important for the interaction of eIF2B with eIF2

natural history study on VWM, including clinical, neuro-imaging, and genetic data (Hamilton et al., 2018).

2.2 | Study population and mutation classification

The natural history study comprised 296 genetically proven VWM patients from 261 families (Hamilton et al., 2018). Reference sequences of *EIF2B1, EIF2B2, EIF2B3, EIF2B4,* and *EIF2B5* are NM_001414.3, NM_014239.3, NM_020365.3, NM_0010341161.1, and NM_003907.2, respectively. In the natural history study, patients were categorized into six different age of onset groups that represent phenotypes of differing severity: antenatal-early infantile disease with onset <1 year (group 1), late-infantile disease with onset between 1 and <2 years (group 2), early-juvenile disease with onset between 2 and <4 years (group 3), juvenile

disease with onset between 4 and <8 years (group 4), late-juvenile to adolescent disease with onset between 8 and <18 years (group 5), and adult disease with onset ≥18 years (group 6) (Hamilton et al., 2018). Based on the information (a) that the clinical parameter age of onset has proven to be the only consistent independent predictor of overall disease severity (Fogli, Schiffmann, Bertini, et al., 2004; Hamilton et al., 2018), (b) that there is a strong genotype–phenotype correlation (Fogli, Schiffmann, Bertini, et al., 2004; van der Lei et al., 2010), and (c) that both missense mutations contribute to disease severity (van der Lei et al., 2010), we used the six previously defined age of onset groups to grade the severity of individual missense mutations. Patients with one or two other mutation types, such as intronic variants or deletions, were omitted from the mutation classification. For the missense variants, we distinguished four severity categories, A–D, using a mathematical, outward-inward, step-by-step approach, A being associated with the most severe

phenotypic effect ("ultra-severe"), B with a "severe" phenotypic effect, C with an "intermediate" phenotypic effect, and D with the mildest phenotypic effect ("mild"). We first gave all homozygous eIF2B missense mutations a severity score of 1–6 on the basis of the calculated mean age of onset group score of the patients with this mutation. Scores obtained in this step were subsequently applied to calculate a score for other variants that occurred in the compound heterozygous state with the already scored variants, depending on the severity scores of the patients who carry both variants. We then determined the numerical score of additional heterozygous variants that occurred in the compound heterozygous state with scored variants. As final step, we translated the calculated numerical scores attributed to the mutations into the four mutation severity categories defined above as follows: score ≤1: category A; score 2–3: category B; score 4: category C; and scores ≥5: category D. In the case of a combination of two different mutations that were each observed only once, it was not possible to achieve a severity category for these mutations and these variants were left out.

2.3 | Benign variants to model

We searched for benign variants in online databases (1000 Genomes, ESP, GnomAD, and dbSNP). We filtered for exonic missense variants with either minor allele frequency >0.001 and more than one homozygote or minor allele frequency of >0.05.

2.4 | Homology modeling

Three structures of the eIF2B decameric complex were identified in the Protein Data Bank: yeast *S. pombe* eIF2B structure (PDB code 5B04, solved by X-ray diffraction, resolution 2.99 Å) (Kashiwagi et al., 2016) and two *H. sapiens* eIF2B structures (6CAJ and 6EZO, solved by cryo-electron microscopy, at resolutions of 2.8 and 4.1 Å, respectively) (Tsai et al., 2018; Zyryanova et al., 2018). Additionally, the crystal structure of human eIF2Bα was identified (PDB code 3ECS, resolution of 2.65 Å) (Hiyama et al., 2009). Analysis of the primary sequences for each subunit revealed that the yeast structure 5B04 has the best sequence coverage, but that the sequence identity between *S. pombe* and human eIF2B is only 32%–48%, depending on the subunit (Table S1) (Tsai et al., 2018). In all three eIF2B structures, yeast, and human, large portions of the N-terminus of eIF2Bδ and the C-terminus of eIF2Bε are missing. The human structures 6CAJ and 6EZO have more gaps than the yeast structure, especially in subunits α and γ. In 6CAJ, a large portion of the C-terminus of eIF2Bγ is absent, including an important I-patch domain, in which VWM mutations occur, and there are many gaps in

flexible regions (e.g., loops), as well as numerous missing side-chains, especially in I-patches in eIF2Bε, where only the positions of backbone atoms have been fitted (Tsai et al., 2018).

We selected 6CAJ, the human eIF2B structure with the best resolution, as a starting point. We used modeling methodologies to fill the many structural gaps. If a template was available, the missing loops were modeled using structure 6EZO as our preferred human template, and 5B04 as a "less preferred" yeast structure. If no suitable template was available, gaps were modeled using the de novo loop modeling tool in Molecular Operating Environment (MOE) version 2017 (MOE, Montreal, QC, Canada; https://web.archive.org/web/20190113221313/http://www.chemcomp.com/MOE-Molecular_Operating_Environment.htm). Very large missing loops were omitted due to the lack of knowledge about their structure. Since the structure of γ I-patch (residues 342–444) was lacking in 6CAJ but not in 6EZO, it was also modeled. The corresponding γ-subunits were aligned, superimposed, and I-patch was transferred to the model based on 6CAJ structure. Missing side-chains were added and other inaccuracies were addressed using the Structure Preparation tool in MOE. Hydrogen atoms were added, protonation states were assigned using Protonate3D in MOE, and the derived structure was charged using Amber10 force field (Case et al., 2008). In order to remove possible clashes between side-chains, the structure was slightly minimized with restraining atoms to the initial coordinates. The final model was named "model_6CAJ."

A separate structure of the human eIF2B catalytic domain (residues 548–721, PDB code 3JUI, resolution 2.0 Å) was also available (Wei et al., 2010), but structural information regarding the residues connecting the catalytic domain with the rest of eIF2Bε was lacking (missing residues 467–547). For this reason, it was considered separately in our study.

2.5 | Location of mutations in the 3D protein structure

The missense mutations, which had been assigned to a severity category, were mapped onto the generated structural model for human eIF2B. Amino acid substitutions were created in WinCoot (version 0.8.9) (Emsley et al., 2010) and the model was refined by optimizing geometric restraints, minimizing free energy, and refining clashing side-chains using ICM-Pro (version 3.8-7b). PyMOL (version 2.2.3, 2020) was used to analyze the in silico models and to create figures. The mutated amino acids were classified depending on their location into specific functional domains, that is, NT-domain (amino acids 4–140 of human eIF2Bγ and 44–165 of eIF2Bε), I-patch (amino acids 334–409 of eIF2Bγ and 347–437 of eIF2Bε), and catalytic domain (amino acids 547–721

of eIF2Bε); the remaining amino acids were assigned to the category "other." They were also classified according to the location of that amino acid in the eIF2B 3D structure, for example, subunit interface, core of a subunit, or exposed to the outer protein surface. Some amino acids could not be modeled onto the structure due to the absence of a template.

3 | RESULTS

3.1 | Mutations and subunits

The *EIF2B1-5* mutations of all 296 patients, their ages of onset, and survival are listed in Table S2. Of these patients, 5 had mutations in the α-subunit, 49 in the eIF2Bβ, 23 in eIF2Bγ, 22 in the δ-subunit, and 197 in the eIF2Bε. Most patients were compound heterozygous ($n = 178$). Forty-two patients had a mutation other than a missense mutation and were excluded from this study. The remaining 254 patients with two missense mutations were available for the classification of individual missense mutations.

The total number of different missense mutations was 127, 5 affecting the α-subunit, 13 eIF2Bβ, 17 eIF2Bγ, 17 the δ-subunit, and 75 eIF2Bε. The total number of different mutation combinations was 157. Twenty-four missense mutations were only observed in combination with another type of mutation and were not scored. There were three patients with two unique missense mutations that could both not be scored for severity (in total six mutations). The remaining 97 different missense mutations were classified into ultra-severe (A, 40 mutations), severe (B, 23), intermediate (C, 13), and mild (D, 21) (Figure 2, Table S3). Of the 97 mutations, 2 affected eIF2Bα, 11 eIF2β, 11 eIF2Bγ, 13 eIF2Bδ, and 60 the ε-subunit. In seven cases, different missense mutations affected the same residue (Table S4): in five, the mutation severity scores were the same or adjacent; in two, the different mutations had dissimilar severity scores.

3.2 | Human eIF2B model

We observed substantial differences between the two human structures (6CAJ and 6EZO, RMSD ~ 2.61 Å, Figure 3a,b), especially in the γ- and ε-subunits, which contain numerous loops and non-resolved regions. Using the human eIF2B structure 6CAJ as main template and filling the gaps by a combination of homology and de novo modeling, a final structure was developed, referred to as "model_6CAJ" (Slynko et al., 2020), which gives a holistic overview of the general arrangement of the subunits and provides information about side-chain orientations and interactions between residues (Figure 3d). The structure of the human catalytic domain is known (Boesen et al., 2004; Wei et al., 2010), but experimental evidence concerning the location of this domain relative to the rest of the complex is lacking. Comparing model_6CAJ to its template PDB structure 6CAJ, overall root-mean-square deviation (RMSD) of atomic positions of 0.26 Å was very low (Figure 3d,e). When comparing the three experimental eIF2B structures (5B04, 6CAJ, and 6EZO) and model_6CAJ to each other, we found, as expected, that the differences between the yeast and the human structures are the largest (RMSD >4 Å, Figure 3b,c,e), likely because their sequence identity is low (35% on average, see also Table S1).

3.3 | Mutations and the 3D protein structure

The 97 missense mutations which were assigned to a severity class were mapped onto the generated model of human eIF2B and color-coded according to their classification (Table S3). Four mutations could not be modeled as these located to regions that were not covered in the 3D structure. In total, 93 mutated residues were investigated in the eIF2B structure. For some cases, more than one mutation affected the same residue (Table S4). Regarding functional domains, 26% of the mutated amino acids were located in NT domains, 11%
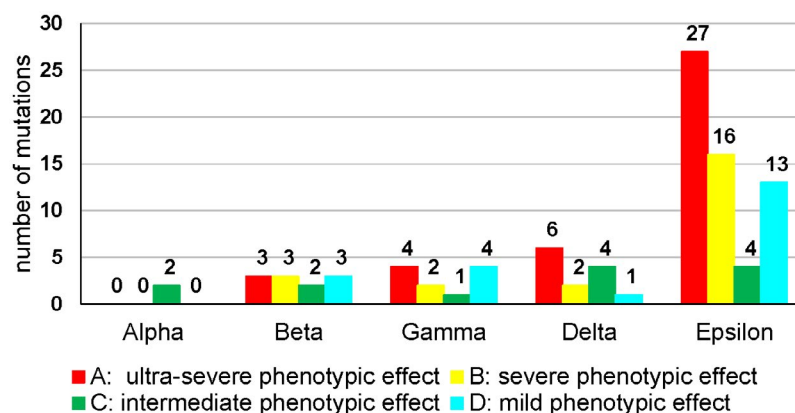

FIGURE 2 Number of variants found in each subunit and classification by severity. The figure presents the sum of corresponding values in Table S2
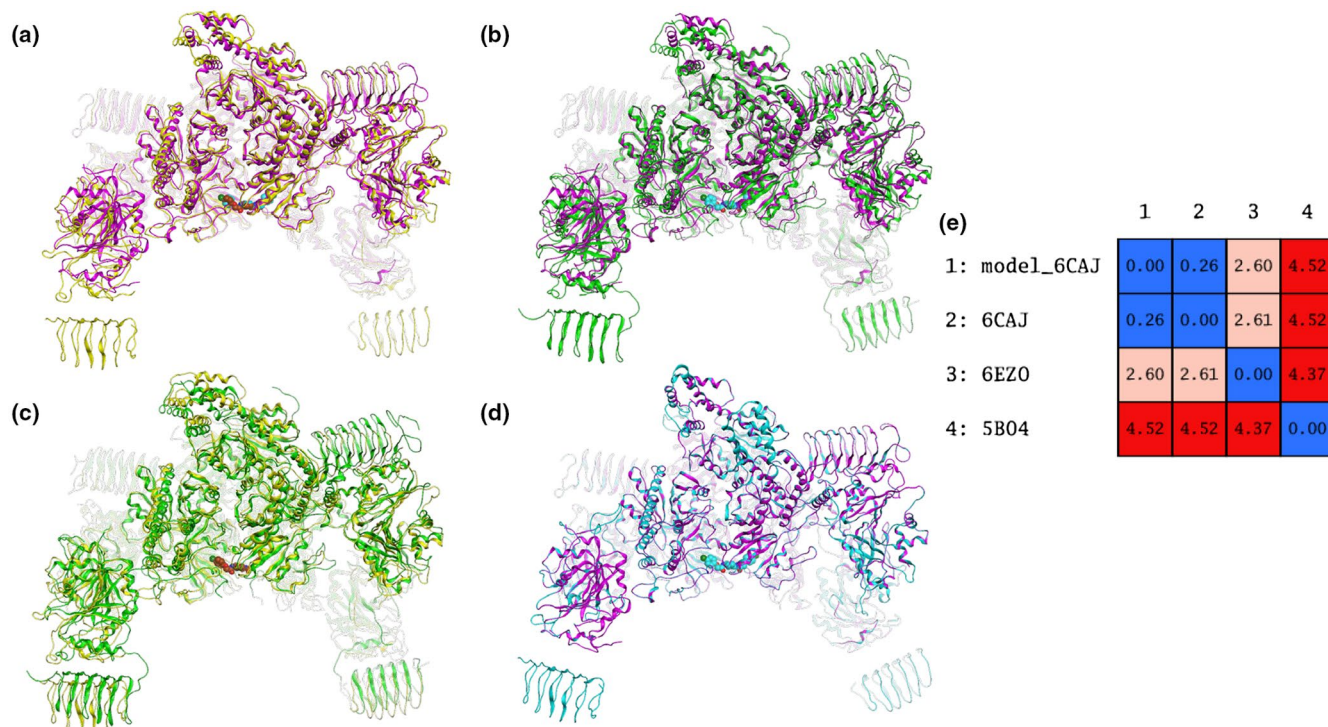
FIGURE 3 CryoEM structures of yeast and human eIF2B. Superpositions are shown of (a) the two human eIF2B structures: 6CAJ (*H. Sapiens*, ribbon in magenta, ligand spheres in cyan) and 6EZO (*H. Sapiens*, ribbon in yellow, ligand spheres in brown); (b) the yeast and the human eIF2B structures: 5B04 (*S. pombe*, ribbon in green) and 6CAJ (*H. Sapiens*, ribbon in magenta, ligand spheres in cyan); (c) the yeast and the human eIF2B structures: 5B04 (*S. pombe*, ribbon in green) and 6EZO (*H. Sapiens*, ribbon in yellow, ligand spheres in brown); and (d) the model_6CAJ (*H. Sapiens*, ribbon in cyan) and its template 6CAJ (*H. Sapiens*, ribbon in magenta, ligand spheres in cyan). (e) Pairwise root mean square deviation (RMSD, in Ångström) between the four structures calculated for Cα atoms in MOE

in I-patches, 7% in the catalytic domain, 0% in the NF motif, and 56% of the mutated amino acids were located elsewhere (Figure 4). Regarding the locations of the amino acids in the 3D structure of eIF2B, 55% of the mutations were located in the interior of protein subunits ("core"), 36% at subunit interfaces, and 5% on the external surface of the complex (Figure 4).

The two human structures of eIF2B (6EZO and 6CAJ) contain a ligand-binding site for the small molecule ISRIB (abbreviation for "integrated stress response inhibitor") (Tsai et al., 2018), which is located at the tetrameric interface of subunits eIF2Bβ and eIF2Bδ (Figure 5a,b). ISRIB is known to stabilize the eIF2B decamer (Zyryanova et al., 2018) and increase its activity (Sidrauski et al., 2015). Two missense mutations were found within high proximity to the ISRIB-binding site: Glu213 in eIF2Bβ and Arg483 in eIF2Bδ (see Figure 5c,d), suggesting that these missense mutations might interfere with ISRIB binding, hampering its effect.

The impacts of the 93 mutations on the eIF2B structure were analyzed and interpreted by superimposing the wild-type eIF2B complex and in silico model of the mutant in PyMOL. Surrounding side-chains of residues within 5 Å of the missense mutation were visualized to identify changes to intramolecular contacts. Loops and secondary structure surrounding the location of the mutant relative to the wild-type

structure were assessed to identify predicted changes to local structure. The results are summarized in Table S5.

3.4 | In vitro biochemical effects of eIF2B mutations

In total, 72 mutations that have been characterized biochemically were investigated regarding their location in the eIF2B 3D structure (Table S6). Of these, 38 are associated with VWM and 21 of the 38 are classified in this study; 34 have not been reported in VWM patients. These 21 mutations were used to assess whether they impact complex stability or GEF activity (i.e., GDP release; Tables S5 and S6). These two parameters provide structural and functional information that can support the interpretation of the effect of mutations in relation to clinical impact. For instance, we can assess whether mutations that reduce the stability of eIF2B complexes in biochemical assays are predicted to be located at the interface between two eIF2B-subunits, with a potential negative impact on the local structure (e.g., eIF2Bβ [Pro291Ser], Table S6). When interpreting these 21 mutations, those associated with unaffected GEF activity were given less weight than those with reduced GEF activity, as the biochemical assay may not fully recapitulate the physiological conditions under which eIF2B is exchanging GDP for GTP on eIF2.
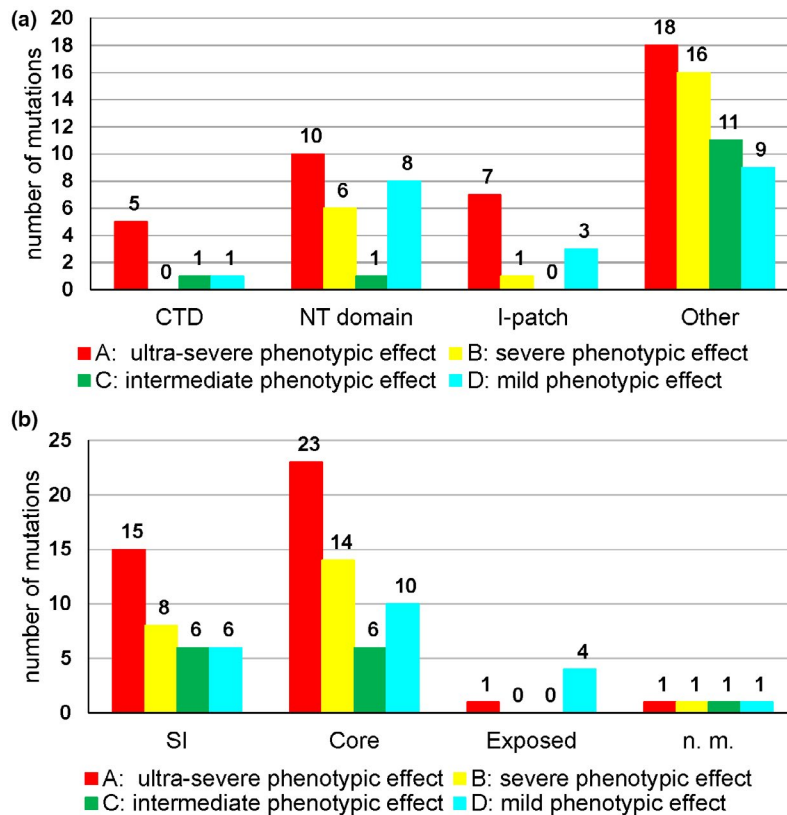
FIGURE 4 Number of variants for functional domains and location in the 3D structure of human eIF2B. Note that some amino acids are affected by several different variants (Table S4) and that four missense mutations are located in regions for which structural information is lacking (n.m. = not modeled), so the total number of classified mutations in the structure is 93 instead of 97. CTD, catalytic domain; SI, subunits interface

3.5 | Correlation between affected subunit and phenotype

The majority of mutations affect the ε-subunit (Figure 2). Indeed, the number of mutations is disproportionately high for its size: of the 97 mutations that were assigned a severity category, 60 affect eIF2B5ε (8.3% of 721 amino acids), 13 affect eIF2Bδ (1.8% of 523 amino acids), 11 affect eIF2Bγ (2.4% of 452 amino acids), 11 affect eIF2Bβ (3.1% of 351 amino acids), and only 2 affect eIF2Bα (0.6% of 305 amino acids). More than half of the 97 mutations have ultra-severe or severe phenotypic effects, with 41% of all mutations classified as "A" and 24% as "B." eIF2Bε and eIF2Bδ contain somewhat higher proportion of class A and class B mutations than eIF2Bγ and eIF2Bβ, while eIF2Bα does not contain any such mutation.

3.6 | Correlation between affected structural domain and phenotype

Most mutations (55%) are located within the 3D structure of eIF2B subunits and affect the "core" (Figure 4b). These mutations are associated with a variable clinical severity (Figure 4b, Table S5). Many mutations (36%) are located at

the interfaces of interacting subunits (Figure 4b), the majority of which have a high severity score (66% of mutations at subunit interfaces have severity score A or B). Virtually no VWM mutations occur in the external surface of the protein complex (Figure 4b).

3.7 | Correlation between genotype and phenotype

In the analysis of the genotype–phenotype correlation, part of the mutations expected to have multiple or very substantial effects on the structure were indeed associated with severe phenotypes (e.g., eIF2Bε [Thr79Ile], [Glu81Leu], [Arg136His], [Arg195His], [His269Pro], [Arg316Gln]; eIF2Bδ [Arg264Trp], [Arg357Trp], [Arg483Trp]; eIF2Bγ [Arg91His]) (Figure 6). Most mutations with predicted small effects on the eIF2B structure or with a conservative change in amino acid were associated with milder disease severity (e.g., eIF2Bε [Thr91Ala] and eIF2Bβ [Glu213Gly]; Figure 7).

However, some mutations with predicted large effects were linked to mild disease, such as eIF2Bε [Arg133His] and eIF2Bβ [Ser171Phe] (Figure 8c), while certain mutations with predicted small effects, for example, eIF2Bβ
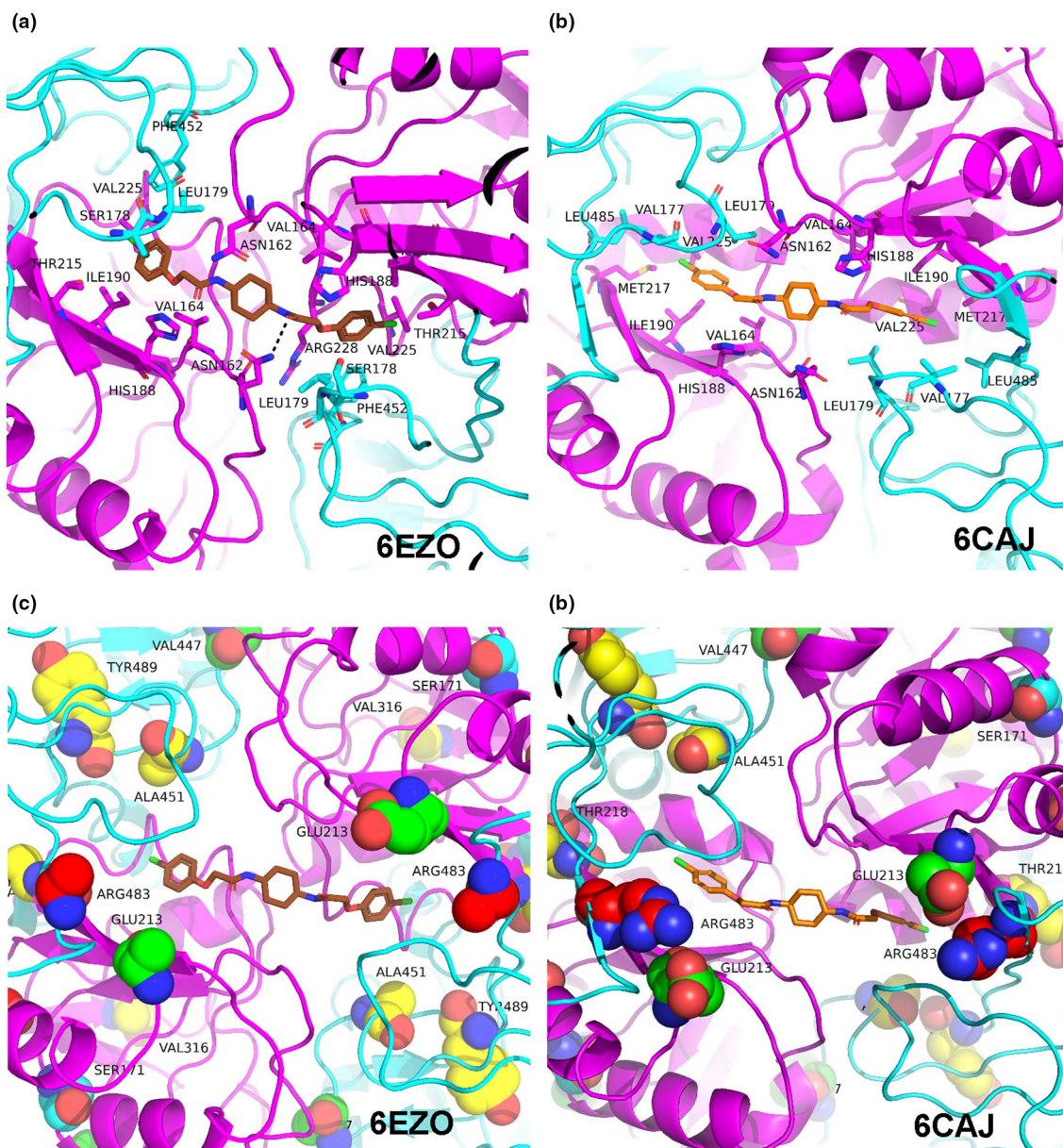
FIGURE 5 Binding site of ligand ISRIB in cryoEM structures 6EZO and 6CAJ. The coloring of subunits was kept consistent with Figure 1. The ligand (depicted as brown/orange sticks on structures 6EZO/6CAJ) binds at the tetrameric interface formed by the two subunits eIF2Bβ (magenta ribbon) and two eIF2Bδ (cyan ribbon). Figures (a) and (b) show binding site residues located 4 Å near ligand ISRIB (note: cryoEM structures 6EZO and 6CAJ have missing side-chains for some residues), whereas figures (c) and (d) depict the locations of eIF2B mutations discussed and classified in this article (see Table S3). The mutated residues are shown as spheres and are colored by severity type

[Gly200Val] and eIF2Bε [Gly386Val], [Ala403Val] and [Thr432Ile], were associated with severe disease (Figure 8, Table S5). Investigation of the latter mutations at the RNA level with Alamut Visual software (version 9, Interactive Biosoftware, France) revealed that the mutations in eIF2Bε are predicted to affect mRNA splicing, causing exon skipping, and expression of eIF2Bε proteins with an internal deletion. Specifically, eIF2Bε [Gly386Val], inactivating the splice donor site at exon 7/intron 8, needs to be renamed into c.1157G>T, p.? (Richards et al., 2015; Wallis et al., 2013).

3.8 | Different mutations affecting the same amino acid residue

Several mutations affect the same residue (Table S4), but result in its change to a different amino acid. In five of these mutations, the severity scores are the same or similar, independent of the amino acid changes (e.g., eIF2Bε [Arg269 to Gly, Pro, or Gln] and eIF2Bε [Arg315 to Gly, Cys, or His]). In two cases, (eIF2Bδ [Arg357Trp/Gln] and eIF2Bε [Val73Met/Gly]), the different mutations have dissimilar severity scores. Interestingly, the predicted effects on the 3D structure (Table

S5) differ for these two mutations. It appears in these two cases that if the amino acid of the mutation has a bulkier or more hydrophobic side-chain than the wild-type residue, there is a stronger effect on disease severity.

3.9 | Benign variants

The search for benign variants yielded five (Table S7). The [Ile587Val] variant is located in the catalytic domain of eIF2Bε and the [Val59Ala] and [Ser404Ala] variants are both located in a region of poor electron density where the side-chains were

not modeled in the wild-type structure. They were, therefore, not modeled in the 3D structure. Modeling the remaining four of these variants in the 3D model predicts minimal local effects to the eIF2B structure (Figure 9). These missense mutations appear to incur no loss or gain of notable polar interactions between side-chains and neighboring residues.

4 | DISCUSSION

The strong genotype–phenotype correlation in VWM has been known for some time (Fogli, Schiffmann, Bertini, et al.,
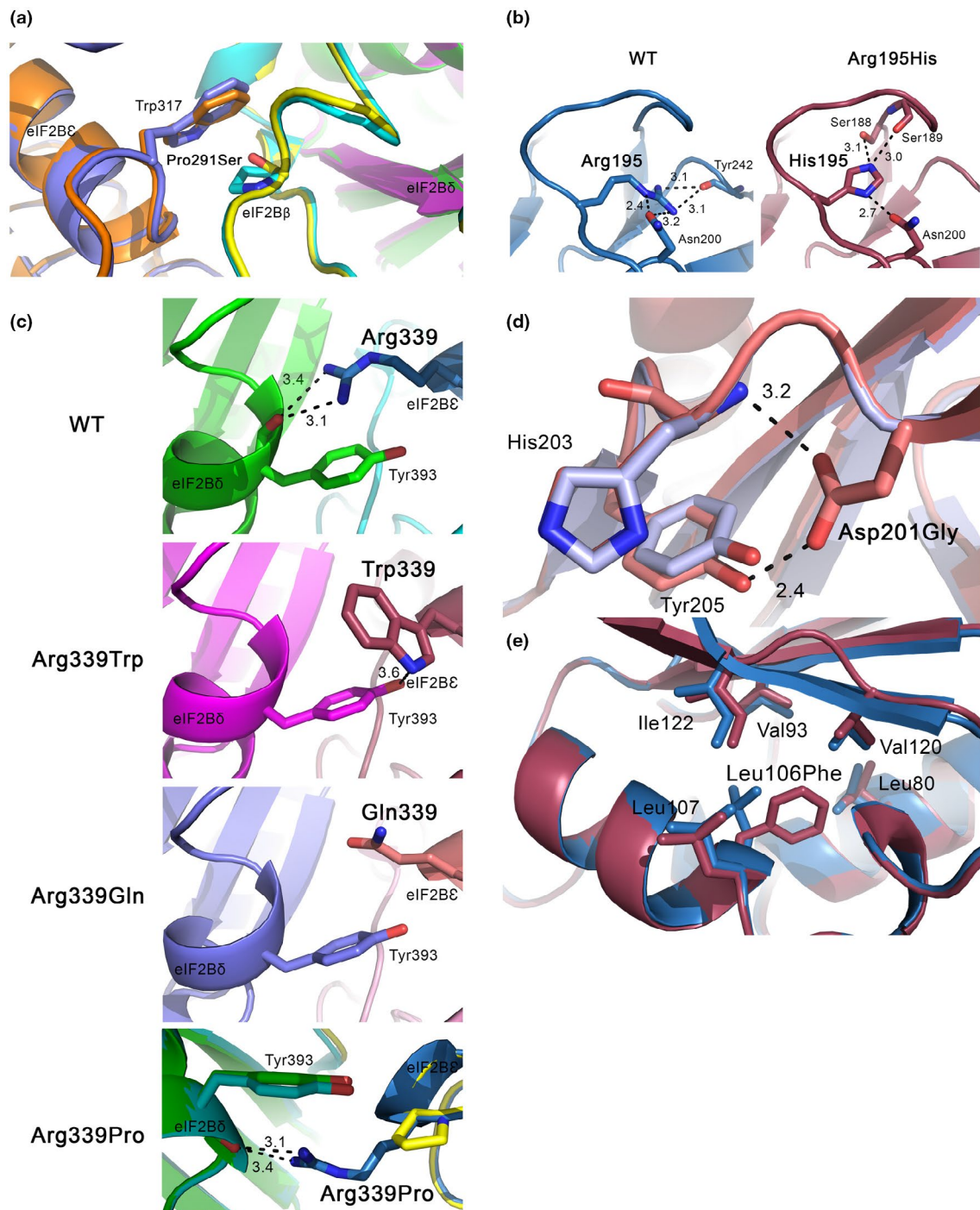
FIGURE 6 Mutations with severe disease severity scores A or B show substantial impact on local structure. (a) Mutation Pro291Ser located on the eIF2Bβ-subunit. The wild-type eIF2Bβ, eIF2Bε-, and eIF2Bδ-subunits are represented in cyan, orange, and green, respectively, and the modeled Pro291Ser mutant eIF2Bβ, eIF2Bε-, and eIF2Bδ-subunits in yellow, purple, and magenta. The modeled mutation predicts a small change in the loop containing Pro291Ser that may affect binding to neighboring subunits, eIF2Bε and eIF2Bδ. The disease score for the mutation is A. (b) Mutation Arg195His located on the eIF2Bε-subunit. The Arg195 on the wild-type eIF2Bε-subunit forms extensive hydrogen bond interactions with the backbone oxygen of Tyr242 and the Asn200 side-chain. In the Arg195His mutant, it is predicted that substitution from Arg to His retains the interaction with Asn200, abolishes the interaction with Tyr242 and introduces new hydrogen bonds with the backbone oxygen atoms of Ser188 and Ser189. Changes to this H-bond network may alter the conformation of this loop. Hydrogen bond interactions are depicted as dotted black lines and all distances are reported in Å. The disease score for the mutation is A. (c) Mutation Arg339Trp, Arg339Gln and Arg339Pro are located on the eIF2Bε-subunit. The Arg339 on the wild-type eIF2Bε-subunit forms hydrogen bond interactions with the backbone oxygen of Tyr393 on eIF2Bδ. In the Arg339Trp mutant, it is predicted that substitution from Arg to Trp abolishes existing interactions and introduces a new hydrogen bond or electrostatic interaction with the side-chain of Tyr393 on eIF2Bδ. In the Arg339Gln mutant, all hydrogen bond interactions are predicted to be abolished. Hydrogen bond interactions are depicted as dotted black lines and all distances are reported in Å. Superimposing Arg339Pro mutant model (eIF2Bδ in cyan and eIF2Bε in yellow) onto the wild-type eIF2B (eIF2Bδ in green and eIF2Bε in blue) shows a predicted change in the secondary structure where the helix-3 is predicted to change to a loop. Due to the location of the mutation, substitution from Arg to Trp, Gln or Pro may affect subunit interactions between eIF2Bδ and eIF2Bε. The disease score for the three mutations is A. (d) Mutation Asp201Gly located on the eIF2Bγ-subunit. The wild-type subunit is represented in salmon and the modeled Asp201Gly mutant in lavender. Substitution of Asp to Gly is predicted to abolish existing hydrogen bond interactions (represented as black dotted lines with distances in Å) with the main chain nitrogen of His203 and the Tyr205 side-chain. Hence, this may introduce flexibility in this region of eIF2Bγ. The disease score for the two mutations is B. (e) Mutation Leu106Phe located on the eIF2Bε-subunit. The wild-type subunit is represented in blue and the modeled Leu106Phe in maroon. Substitution from Leu to Phe may promote favorable hydrophobic interactions with surrounding residues (labeled). However, substitution to a large and bulky side-chain may affect folding in this region of eIF2Bε. The disease score for the two mutations is B. Protein sequences are based on reference sequences NM_001414.3 (*EIF2B1*), NM_014239.3 (*EIF2B2*), NM_020365.3 (*EIF2B3*), NM_0010341161.1 (*EIF2B4*), and NM_003907.2 (*EIF2B5*)
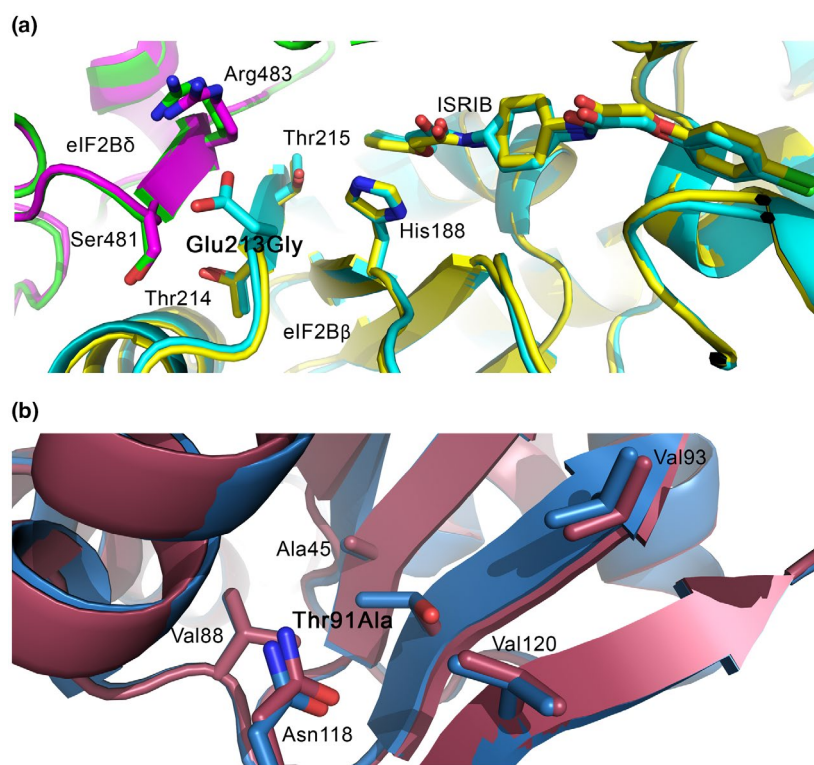

FIGURE 7 Mutations with disease severity category C show small impact on local structure. (a) Mutation Glu213Gly located on the eIF2Bβ-subunit. The wild-type eIF2Bβ and eIF2Bδ are represented in cyan and purple, respectively, and the modeled Glu213Gly mutant eIF2Bβ and eIF2Bδ in yellow and green. Due to the location of the mutation, substitution from Glu to Gly may affect subunit interactions between eIF2Bβ and eIF2Bδ. It also lies close to the binding site occupied by the integrated stress response inhibitor (ISRIB). The disease score for the mutation is C. (b) Mutation Thr91Ala located on the eIF2Bε-subunit. The wild-type subunit is represented in blue and the modeled Thr91Ala in maroon. Substitution from Thr to Ala may promote favorable hydrophobic interactions with surrounding residues, Ala45, Val88, Val93, and Val120 (labeled) and is predicted to only have a small effect on structure. The disease score for the mutation is C. Protein sequences are based on reference sequences of NM_014239.3 (*EIF2B2*), NM_0010341161.1 (*EIF2B4*), and NM_003907.2 (*EIF2B5*)
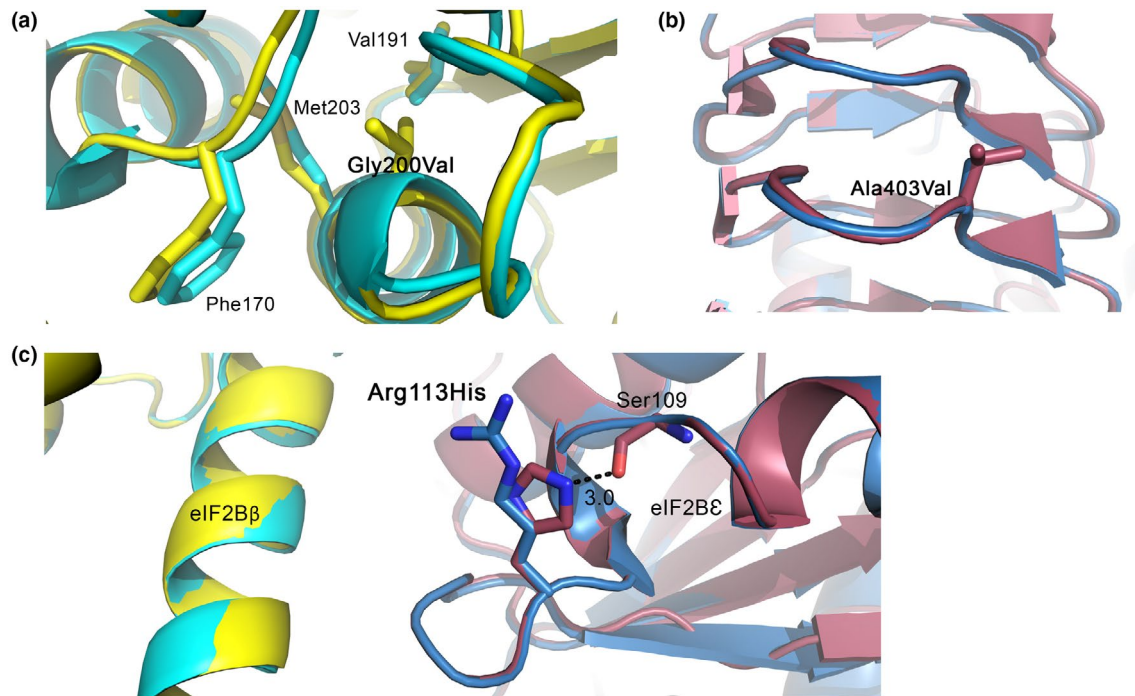
FIGURE 8 Mutations with predicted structural effects not matching disease severity. (a) Mutation Gly200Val located on the eIF2Bβ-subunit where the wild-type structure is represented in cyan and the modeled Gly200Val mutant in yellow. Substitution from Gly to Val might promote hydrophobic interactions with adjacent residues (labeled). The model predicts small, localized changes in the structure of eIF2Bβ. The disease severity category for the mutation is A. (b) Mutation Ala403Val located on the eIF2Bε-subunit. The wild-type eIF2Bε-subunit is represented in blue and the modeled Ala403Val mutant eIF2Bε-subunit in maroon. The Ala403Val residue is located on a solvent-exposed, flexibly loop. Due to the similar chemical nature of Ala and Val, this mutation is predicted to have a small effect on loop conformation. The severity category for the mutation is A. (c) Mutation Arg113His located on the eIF2Bε-subunit. The wild-type eIF2Bε- and eIF2Bβ-subunits are represented in blue and cyan, respectively, and the modeled Arg113His mutant eIF2Bε- and eIF2Bβ-subunits in maroon and yellow. Substitution of Arg to His is predicted to introduce a hydrogen bond interaction with the backbone oxygen of Ser109 (represented as black dotted lines with distances in Å). The location of the Arg113His mutation occurs in a region close to the eIF2Bβ-subunit. The severity category for the mutation is D. Protein sequences are based on reference sequences of NM_014239.3 (*EIF2B2*) and NM_003907.2 (*EIF2B5*)

2004; van der Lei et al., 2010), but remains unexplained. No clear correlation has been observed between the GEF activity of mutated complexes, measured in vitro, and clinical disease severity (Liu et al., 2011). We located the mutations in a structure of eIF2B and assessed whether specific locations are associated with clinical disease severity and known biochemical effects.

For the interpretation of findings in our study, it is important to realize that the number of known benign missense variants, which have not been associated with any clinical disease, is extremely low (Table S7; 0–2 per subunit), indicating that variants in *EIF2B1–5* are not easily tolerated and readily cause a clinical phenotype. It is also important to realize that eIF2B is an essential protein complex and that homozygous variants in the corresponding genes that are incompatible with life are, therefore, missed. Thus, the most severe end of the spectrum is very likely incompletely inventoried.

Our data confirm previous findings, indicating that the majority of mutations affect the ε-subunit and that eIF2Bε contains the highest proportion of class A and class B mutations. When contemplating the explanation for the

disproportionately high number of mutations in the ε-subunit and their often (ultra)-severe phenotypic effect in patients, it helps to consider that the proportion of mutations compared to its size is lowest in eIF2Bα, and that no mutations with severe or ultra-severe effect are seen in this subunit, although the overall low number of mutations in eIF2Bα precludes firm conclusions. Yeast knock-outs for any of the subunit genes are non-viable, apart from eIF2Bα (Hannig & Hinnebusch, 1988). Complexes lacking the α-subunit still have 50% of biochemical activity (Liu et al., 2011). Biochemical data that show that the eIF2Bε-subunit containing the catalytic domain has 10% of the biochemical activity found with the eIF2Bα-ε pentamer (Liu et al., 2011; data not shown). In addition, the yeast eIF2Bε-subunit is essential for displacing eIF5 from eIF2, making eIF2 available for exchanging GDP for GTP (Singh et al., 2006). Although for human eIF2B this function still needs to be explored, it is likely, based on the high similarity of the three initiation factors involved, that these steps also occur in mammalian cells. All the above considerations suggest that eIF2Bε is the most important subunit for eIF2B function, consistent with it containing the catalytic domain,
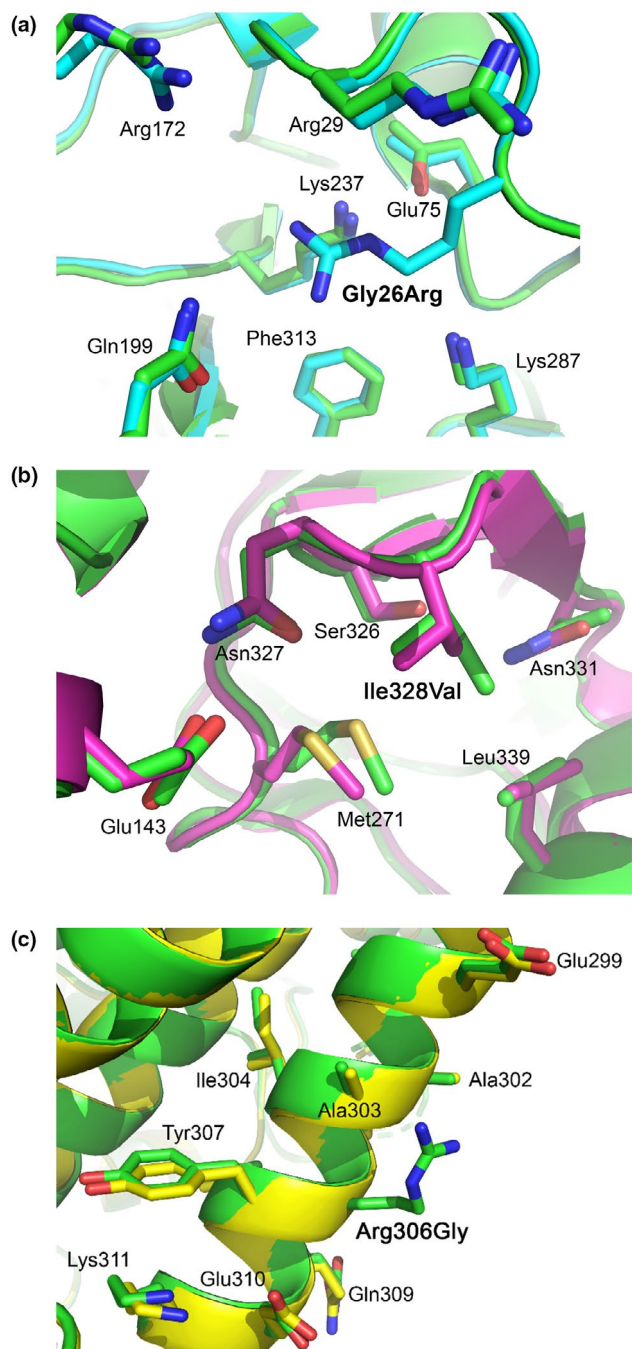
FIGURE 9 Modeling of benign variants show small predicted effects in local structure. The wild-type eIF2B structure (green) is superimposed onto modeled mutant structures (a) Gly26Arg (cyan) located on eIF2Bβ, (b) Ile328Val (magenta) located on eIF2Bβ, (c) Arg306Gly (yellow) located on eIF2Bδ, and (d) Ala127Val (purple) located on eIF2Bβ. Modeling of the benign variants shows no predicted loss or gain of polar interactions with neighboring residues. Protein sequences are based on reference sequences NM_014239.3 (*EIF2B2*) and NM_0010341161.1 (*EIF2B4*)

and most vulnerable to the effects of mutations, while eIF2Bα is least important.

We created a 3D model of human eIF2B to investigate if mutations causing various disease severities clustered in

particular regions of the structure of the eIF2B complex. In agreement with work from others, we found that VWM-causing mutations localize in many different regions of the eIF2B complex (Kashiwagi et al., 2016). Previous work did not systematically take disease severity into account. Regarding functional domains, the current study shows that almost all mutations in the catalytic domain are ultra-severe. Strikingly, most mutations are found outside known functional domains, reflecting that eIF2B structure is poorly described and not well-understood in terms of its function or interacting protein partners, and that simply sorting mutations by their involvement in functional domains often does not explain why some of mutations cause more severe disease effects than others.

Most mutations in this study (55%) affect the "core" of eIF2B subunits and have variable impact on clinical severity. Most likely, many of the severe mutations located in subunit cores are connected to eIF2B function and some of them are very probably important for the correct folding of subunits. Many mutations in this study (36%) are located at the interfaces of interacting subunits and the majority of them have a high severity score. These amino acids play a pivotal role in complex formation and thus in the function and perhaps regulation of eIF2B. Virtually no VWM mutations occur in the external surface of the eIF2B complex, perhaps because any mutations that occur in such positions have little effect on the function of eIF2B and do not result in a phenotypic change. One mutation that is predicted to be exposed on the external surface is eIF2Bδ [Pro243Leu]; interestingly, this location has recently been implicated in binding eIF2, which likely explains the high severity score for the mutation (Kashiwagi et al., 2019).

Overall, the correlation of disease severity with location of the mutation within the eIF2B model is not perfect. Some mutations with predicted substantial effects on eIF2B are indeed associated with severe phenotypes and most mutations with predicted small effects on eIF2B are associated with milder disease severity. For certain mutations with predicted small effects on eIF2B but associated with severe disease, it is likely that they affect mRNA splicing with major effects on the eIF2B subunit protein expression. Some mutations with predicted large effects are linked to mild disease. While these mutations may have a substantial effect on local structure, it is possible that this does not impact the function or stability of eIF2B leading to a mild or moderate phenotype.

X-ray crystallography yields a single structure, which is compatible with crystallization within the lattice of the crystal, and cannot capture the protein's flexibility. At the moment, we cannot precisely predict global changes to protein structure caused by mutations and cannot assess the effects of mutations on the flexibility of the protein structure, which may have a substantial impact on the folding of eIF2B-subunits, holo-complex formation, regulation, and/or function.

To investigate this further, we will need to understand the full repertoire of eIF2B functions and their regulation. Biochemical or cellular assays that investigate these functions and regulation would aid greatly in fully understanding the effect of mutations on eIF2B function. These assays may then become more valuable in diagnosis and clinical trials than is currently the case (Liu et al., 2011). The currently available GEF assays clearly do not reflect functional consequences in all cases and can only be used as a starting point for developing such an overall functional assay. A suitable assay, or set of assays, that reflects all eIF2B functions may well assist in the diagnosis of VWM and in assessing the predicted disease severity associated with novel mutations.

Severity-grading of mutations, insight into genotype–phenotype correlation and knowledge of clinical predictors of outcome improve counseling of patients and families. Reliable mutation-based prediction of the disease course facilitates clinical decision making, for instance in the case of prenatal testing. It is, however, important to realize that the genotype is not the only factor determining the phenotype. The recent natural history study shows that environmental factors also influence disease severity, especially for patients with longer survival (Hamilton et al., 2018). Environmental stresses, like febrile infections and head trauma, negatively impact the disease course. They can in part be avoided by preventive measures, thereby also impacting the phenotype (Hamilton et al., 2018).

Different therapies for VWM are emerging and the first trials are being developed (Abbink et al., 2019; Dooves et al., 2018; Wong et al., 2019). The effects of treatment may be influenced by the mutations of the patient, as indicated for ISRIB (Abbink et al., 2019), requiring individualized therapy decisions. Importantly, considering that VWM is a fatal disease, trials using historical controls may ethically be preferable above placebo-controlled trials. The current study and a previous natural history study (Hamilton et al., 2018) provide the first data needed for propensity score matching, that is, based on age of onset and mutation severity.

CONFLICT OF INTEREST
Dr. van der Knaap and Dr. Abbink have a patent P112686CA00, therapeutic effects of Guanabenz treatment in vanishing white matter, pending to VU University Medical Center Amsterdam. None of the other co-authors has a conflict of interest to declare.

AUTHORS' CONTRIBUTIONS
Marjo S. van der Knaap, Iwan J.P. de Esch, Chris de Graaf, Christopher G. Proud, and Truus E.M. Abbink conceived and designed the study. Inna Slynko performed the in silico modeling to create a new human eIF2B model structure, onto which she mapped the missense mutations. Eline M.C. Hamilton severity-graded the missense mutations. Stephanie Nguyen, Lisanne E. Wisse, John B. Bruning, Christopher G. Proud, and Truus E.M. Abbink assessed the mutated residues for location in subunits, eIF2B complex, and functional domains, and for information on biochemical activity. Marjo S. van der Knaap, Inna Slynko, Christopher G. Proud, and Truus E.M. Abbink wrote the paper, which was critically reviewed and adapted by all coauthors.

DATA AVAILABILITY STATEMENT
The data that support the findings of this study are available in the supporting information of this article. The 6AJ structure model is openly available in Zenodo.org at https://doi.org/10.5281/zenodo.3759412, reference number https://doi.org/10.5281/zenodo.3759412.

ORCID
Inna Slynko https://orcid.org/0000-0003-1628-2834
Stephanie Nguyen https://orcid.org/0000-0003-0989-7734
Eline M. C. Hamilton https://orcid.org/0000-0001-7017-1188
Lisanne E. Wisse https://orcid.org/0000-0002-9367-5730
Iwan J. P. de Esch https://orcid.org/0000-0002-1969-0238
Chris de Graaf https://orcid.org/0000-0002-1226-2150
John B. Bruning https://orcid.org/0000-0002-6919-1824
Christopher G. Proud https://orcid.org/0000-0003-0704-6442
Truus E. M. Abbink https://orcid.org/0000-0001-6932-0449
Marjo S. van der Knaap https://orcid.org/0000-0001-8912-0954

REFERENCES
Abbink, T. E. M., Wisse, L. E., Jaku, E., Thiecke, M. J., Voltolini-González, D., Fritsen, H., Bobeldijk, S., Ter Braak, T. J., Polder, E., Postma, N. L., Bugiani, M., Struijs, E. A., Verheijen, M., Straat, N., van der Sluis, S., Thomas, A. A. M., Molenaar, D., & van der Knaap, M. S. (2019). Vanishing white matter: Deregulated integrated stress response as therapy target. *Annals of Clinical and Translational Neurology*, *6*, 1407–1422.

Boesen, T., Mohammad, S. S., Pavitt, G. D., & Andersen, G. R. (2004). Structure of the catalytic fragment of translation initiation factor 2B and identification of a critically important catalytic residue. *Journal of Biological Chemistry*, *279*, 10584–10592.

Case, D. A., Darden, T. A., Cheatham, T. E., Simmerling, C. L., Wang, J., Duke, R. E., Luo, R., Crowley, M., Walker, R. C., Zhang,

W., Merz, K. M., Wang, B., Hayik, S., Roitberg, A., Seabra, G., Kolossváry, I., Wong, K. F., Paesani, F., Vanicek, J., … Kollman, P. A. (2008). *AMBER 10*. University of California, San Francisco. https://infoscience.epfl.ch/record/121435

Dever, T. E. (2002). Gene-specific regulation by general translation factors. *Cell*, *108*, 545–556.

Dolan, M. A., Noah, J. W., & Hurt, D. (2012). Comparison of common homology modeling algorithms: Application of user-defined alignments. *Methods in Molecular Biology*, *857*, 399–414.

Dooves, S., Bugiani, M., Wisse, L. E., Abbink, T. E. M., van der Knaap, M. S., & Heine, V. M. (2018). Bergmann glia translocation: A new disease marker for vanishing white matter identifies therapeutic effects of Guanabenz treatment. *Neuropathology and Applied Neurobiology*, *44*, 391–403.

Emsley, P., Lohkamp, B., Scott, W. G., & Cowtan, K. (2010). Features and development of Coot. *Acta Crystallographica*, *D66*, 486–501.

Fiser, A. (2010). Template-based protein structure modeling. In D. Fenyö (Ed.), *Computational biology. Methods in molecular biology 673* (pp. 73–94). Humana Press.

Fogli, A., Schiffmann, R., Bertini, E., Ughetto, S., Combes, P., Eymard-Pierre, E., Kaneski, C. R., Pineda, M., Troncoso, M., Uziel, G., Surtees, R., Pugin, D., Chaunu, M. P., Rodriguez, D., & Boespflug-Tanguy, O. (2004). The effect of genotype on the natural history of eIF2B-related leukodystrophies. *Neurology*, *62*, 1509–1517.

Fogli, A., Schiffmann, R., Hugendubler, L., Combes, P., Bertini, E., Rodriguez, D., Kimball, S. R., & Boespflug-Tanguy, O. (2004). Decreased guanine nucleotide exchange factor activity in eIF2B-mutated patients. *European Journal of Human Genetics*, *12*, 561–566.

Gomez, E., & Pavitt, G. D. (2000). Identification of domains and residues within the ε-subunit of eukaryotic translation initiation factor 2B (eIF2B ε) required for guanine nucleotide exchange reveals a novel activation function promoted by eIF2B complex formation. *Molecular and Cellular Biology*, *20*, 3965–3976.

Gordiyenko, Y., Schmidt, C., Jennings, M. D., Matak-Vinkovic, D., Pavitt, G. D., & Robinson, C. V. (2014). eIF2B is a decameric guanine nucleotide exchange factor with a gamma2epsilon2 tetrameric core. *Nature Communications*, *5*, 3902.

Hamilton, E. M. C., van der Lei, H. D. W., Vermeulen, G., Gerver, J. A. M., Lourenço, C. M., Naidu, S., Mierzewska, H., Gemke, R. J. B. J., de Vet, H. C. W., Uitdehaag, B. M. J., Lissenberg-Witte, B. I., VWM Research Group, & van der Knaap, M. S. (2018). The natural history of vanishing white matter. *Annals of Neurology*, *84*, 274–288.

Hannig, E. M., & Hinnebusch, A. G. (1988). Molecular analysis of GCN3, a translational activator of GCN4: Evidence for posttranslational control of GCN3 regulatory function. *Molecular and Cellular Biology*, *8*, 4808–4820.

Hiyama, T. B., Ito, T., Imataka, H., & Yokoyama, S. (2009). Crystal structure of the alpha subunit of human translation initiation factor 2B. *Journal of Molecular Biology*, *392*, 937–951.

Horzinski, L., Huyghe, A., Cardoso, M. C., Gonthier, C., Ouchchane, L., Schiffmann, R., Blanc, P., Boespflug-Tanguy, O., & Fogli, A. (2009). Eukaryotic initiation factor 2B (eIF2B) GEF activity as a diagnostic tool for EIF2B-related disorders. *PLoS One*, *4*, e8318.

Kashiwagi, K., Takahashi, M., Nishimoto, M., Hiyama, T. B., Higo, T., Umehara, T., Sakamoto, K., Ito, T., & Yokoyama, S. (2016). Crystal structure of eukaryotic translation initiation factor 2B. *Nature*, *531*, 122–125.

Kashiwagi, K., Yokoyama, T., Nishimoto, M., Takahashi, M., Sakamoto, A., Yonemochi, M., Shirouzu, M., & Ito, T. (2019). Structural basis for eIF2B inhibition in integrated stress response. *Science*, *364*, 495–499.

Labauge, P., Horzinski, L., Ayrignac, X., Blanc, P., Vukusic, S., Rodriguez, D., Mauguiere, F., Peter, L., Goizet, C., Bouhour, F., Denier, C., Confavreux, C., Obadia, M., Blanc, F., de Sèze, J., Fogli, A., & Boespflug-Tanguy, O. (2009). Natural history of adult-onset eIF2B-related disorders: A multi-centric survey of 16 cases. *Brain*, *132*, 2161–2169.

Leegwater, P. A., Vermeulen, G., Könst, A. A., Naidu, S., Mulders, J., Visser, A., Kersbergen, P., Mobach, D., Fonds, D., van Berkel, C. G., Lemmers, R. J., Frants, R. R., Oudejans, C. B., Schutgens, R. B., Pronk, J. C., & van der Knaap, M. S. (2001). Subunits of the translation initiation factor eIF2B are mutant in leukoencephalopathy with vanishing white matter. *Nature Genetics*, *29*, 383–388.

Leng, X., Wu, Y., Wang, X., Pan, Y., Wang, J., Li, J., Du, L., Dai, L., Wu, X., Proud, C. G., & Jiang, Y. (2011). Functional analysis of recently identified mutations in eukaryotic translation initiation factor 2Bε (eIF2Bε) identified in Chinese patients with vanishing white matter disease. *Journal of Human Genetics*, *56*, 300–305.

Li, W., Wang, X., van der Knaap, M. S., & Proud, C. G. (2004). Mutations linked to leukoencephalopathy with vanishing white matter impair the function of the eukaryotic initiation factor 2B complex in diverse ways. *Molecular and Cellular Biology*, *24*, 3295–3306.

Liu, R., van der Lei, H. D., Wang, X., Wortham, N. C., Tang, H., van Berkel, C. G., Mufunde, T. A., Huang, W., van der Knaap, M. S., Scheper, G. C., & Proud, C. G. (2011). Severity of vanishing white matter disease does not correlate with deficits in eIF2B activity or the integrity of eIF2B complexes. *Human Mutation*, *32*, 1036–1045.

Matsukawa, T., Wang, X., Liu, R., Wortham, N. C., Onuki, Y., Kubota, A., Hida, A., Kowa, H., Fukuda, Y., Ishiura, H., Mitsui, J., Takahashi, Y., Aoki, S., Takizawa, S., Shimizu, J., Goto, J., Proud, C. G., & Tsuji, S. (2011). Adult-onset leukoencephalopathies with VWM with novel missense mutations in *EIF2B2, EIF2B3,* and *EIF2B5*. *Neurogenetics*, *12*, 259–261.

Pavitt, G. D. (2005). eIF2B, a mediator of general and gene-specific translational control. *Biochemical Society Transactions*, *33*, 1487–1492.

Proud, C. G. (2005). eIF2 and the control of cell physiology. *Seminars in Cell & Developmental Biology*, *16*, 3–12.

Reid, P. J., Mohammad-Qureshi, S. S., & Pavitt, G. D. (2012). Identification of intersubunit domain interactions within eukaryotic initiation factor (eIF) 2B, the nucleotide exchange factor for translation initiation. *The Journal of Biological Chemistry*, *287*, 8275–8285.

Richards, S., Aziz, N., Bale, S., Bick, D., Das, S., Gastier-Foster, J., Grody, W. W., Hegde, M., Lyon, E., Spector, E., Voelkerding, K., & Rehm, H. L. (2015). Standards and guidelines for the interpretation of sequence variants: A joint consensus recommendation of the American College of Medical Genetics and Genomics and the Association for Molecular Pathology. *Genetics in Medicine*, *17*, 405–423.

Rowlands, A. G., Panniers, R., & Henshaw, E. C. (1988). The catalytic mechanism of guanine nucleotide exchange factor action and competitive inhibition by phosphorylated eukaryotic initiation factor 2. *The Journal of Biological Chemistry*, *263*, 5526–5533.

Sidrauski, C., Tsai, J. C., Kampmann, M., Hearn, B. R., Vedantham, P., Jaishankar, P., Sokabe, M., Mendez, A. S., Newton, B. W., Tang, E. L., Verschueren, E., Johnson, J. R., Krogan, N. J., Fraser, C. S., Weissman, J. S., Renslo, A. R., & Walter, P. (2015). Pharmacological dimerization and activation of the exchange factor eIF2B antagonizes the integrated stress response. *eLife*, *4*, e07314.

Singh, C. R., Lee, B., Udagawa, T., Mohammad-Qureshi, S. S., Yamamoto, Y., Pavitt, G. D., & Asano, K. (2006). An eIF5/eIF2 complex antagonizes guanine nucleotide exchange by eIF2B during translation initiation. *EMBO Journal*, *25*, 4537–4546.

Slynko, I., de Graaf, C., & de Esch, I. (2020). Homology model of human eIF2B. *Zenodo*. https://doi.org/10.5281/zenodo.3759412

The PyMOL Molecular Graphics System (version 2.2.3). (n.d.). Schrödinger, LLC.

Tsai, J. C., Miller-Vedam, L. E., Anand, A. A., Jaishankar, P., Nguyen, H. C., Renslo, A. R., Frost, A., & Walter, P. (2018). Structure of the nucleotide exchange factor eIF2B reveals mechanism of memory-enhancing molecule. *Science*, *359*, 1483.

van der Knaap, M. S., Pronk, J. C., & Scheper, G. C. (2006). Vanishing white matter disease. *Lancet Neurology*, *5*, 413–423.

van der Knaap, M. S., Leegwater, P. A., Könst, A. A., Visser, A., Naidu, S., Oudejans, C. B., Schutgens, R. B., & Pronk, J. C. (2002). Mutations in each of the five subunits of translation initiation factor eIF2B can cause leukoencephalopathy with vanishing white matter. *Annals of Neurology*, *51*, 264–270.

van der Knaap, M. S., van Berkel, C. G., Herms, J., van Coster, R., Baethmann, M., Naidu, S., Boltshauser, E., Willemsen, M. A., Plecko, B., Hoffmann, G. F., Proud, C. G., Scheper, G. C., & Pronk, J. C. (2003). eIF2B-related disorders: Antenatal onset and involvement of multiple organs. *American Journal of Human Genetics*, *73*, 1199–1207.

van der Knaap, M. S., Bugiani, M., Boor, I., Proud, C. G., & Scheper, G. C. (2010). Vanishing white matter. In D. Valle, S. Antonarakis, A. Ballabio, A. Beaudet, & G. A. Mitchell (Eds.), *The online metabolic and molecular bases of inherited disease (OMMBID)* (chapter 235.1, pp. 1–44). McGraw-Hill.

van der Lei, H. D., van Berkel, C. G., van Wieringen, W. N., Brenner, C., Feigenbaum, A., Mercimek-Mahmutoglu, S., Philippart, M., Tatli, B., Wassmer, E., Scheper, G. C., & van der Knaap, M. S. (2010). Genotype-phenotype correlation in vanishing white matter disease. *Neurology*, *75*, 1555–1559.

Wallis, Y., Payne, W., McAnulty, C., Bodmer, D., Sistermans, E., Robertson, K., Moore, D., Abbs, S., Deans, Z., & Devereau, A. (2013). Practice guidelines for the evaluation of pathogenicity and the reporting of sequence variants in clinical molecular genetics. *Association for Clinical Genetic Science*. https://www.acgs.uk.com/media/10791/evaluation_and_reporting_of_sequence_variants_bpgs_june_2013_-_finalpdf.pdf

Wallner, B., & Elofsson, A. (2005). All are not equal: A benchmark of different homology modeling programs. *Protein Science*, *14*, 1315–1327.

Wang, X., Wortham, N. C., Liu, R., & Proud, C. G. (2012). Identification of residues that underpin interactions within the eukaryotic initiation factor (eIF2) 2B complex. *The Journal of Biological Chemistry*, *287*, 8263–8274.

Wei, J., Jia, M., Zhang, C., Wang, M., Gao, F., Xu, H., & Gong, W. (2010). Crystal structure of the C-terminal domain of the ε-subunit of human translation initiation factor eIF2B. *Protein Cell*, *1*, 595–603.

Williams, D. D., Price, N. T., Loughlin, A. J., & Proud, C. G. (2001). Characterization of the mammalian initiation factor eIF2B complex as a GDP dissociation stimulator protein. *The Journal of Biological Chemistry*, *276*, 24697–24703.

Wong, Y. L., LeBon, L., Basso, A. M., Kohlhaas, K. L., Nikkel, A. L., Robb, H. M., Donnelly-Roberts, D. L., Prakash, J., Swensen, A. M., Rubinstein, N. D., Krishnan, S., McAllister, F. E., Haste, N. V., O'Brien, J. J., Roy, M., Ireland, A., Frost, J. M., Shi, L., Riedmaier, S., … Sidrauski, C. (2019). eIF2B activator prevents neurological defects caused by a chronic integrated stress response. *eLife*, *8*, e42940.

Wortham, N. C., Martinez, M., Gordiyenko, Y., Robinson, C. V., & Proud, C. G. (2014). Analysis of the subunit organization of the eIF2B complex reveals new insights into its structure and regulation. *FASEB Journal*, *28*, 2225–2237.

Wortham, N. C., & Proud, C. G. (2015). Biochemical effects of mutations in the gene encoding the alpha-subunit of eukaryotic initiation factor (eIF) 2B associated with vanishing white matter disease. *BMC Medical Genetics*, *16*, 64.

Zyryanova, A. F., Weis, F., Faille, A., Alard, A. A., Crespillo-Casado, A., Sekine, Y., Harding, H. P., Allen, F., Parts, L., Fromont, C., Fischer, P. M., Warren, A. J., & Ron, D. (2018). Binding of ISRIB reveals a regulatory site in the nucleotide change factor eIF2B. *Science*, *359*, 1533–1536.

SUPPORTING INFORMATION

Additional Supporting Information may be found online in the Supporting Information section.